Research Square

Preprints are preliminary reports that have not undergone peer review.
They should not be considered conclusive, used to inform clinical practice,
or referenced by the media as validated information.

De-inking of surface printing ink on waste polypropylene (PP) milk tea cups using nonionic surfactants

Lijun Xu
Shanghai Polytechnic University
Yue Ning
Shanghai Polytechnic University
Jingwen Xu
Shanghai Polytechnic University
Nuo Xu
Shanghai Polytechnic University
Qing Huang
Shanghai Polytechnic University
Li Zhang
Shanghai Polytechnic University
Jianming Zhu
Shanghai Polytechnic University
Wenyi Yuan
wyyuan@sspu.edu.cn

Shanghai Polytechnic University

Research Article

Keywords: Deinking efficiency, Polypropylene, Nonionic surfactants, Milk tea cup

Posted Date: November 18th, 2026

DOI: https://doi.org/10.21203/rs.3.rs-11549788/v1

License: This work is licensed under a Creative Commons Attribution 4.0 International License.
Read Full License

Additional Declarations: No competing interests reported.

De-inking of surface printing ink on waste polypropylene (PP) milk tea cups using nonionic surfactants

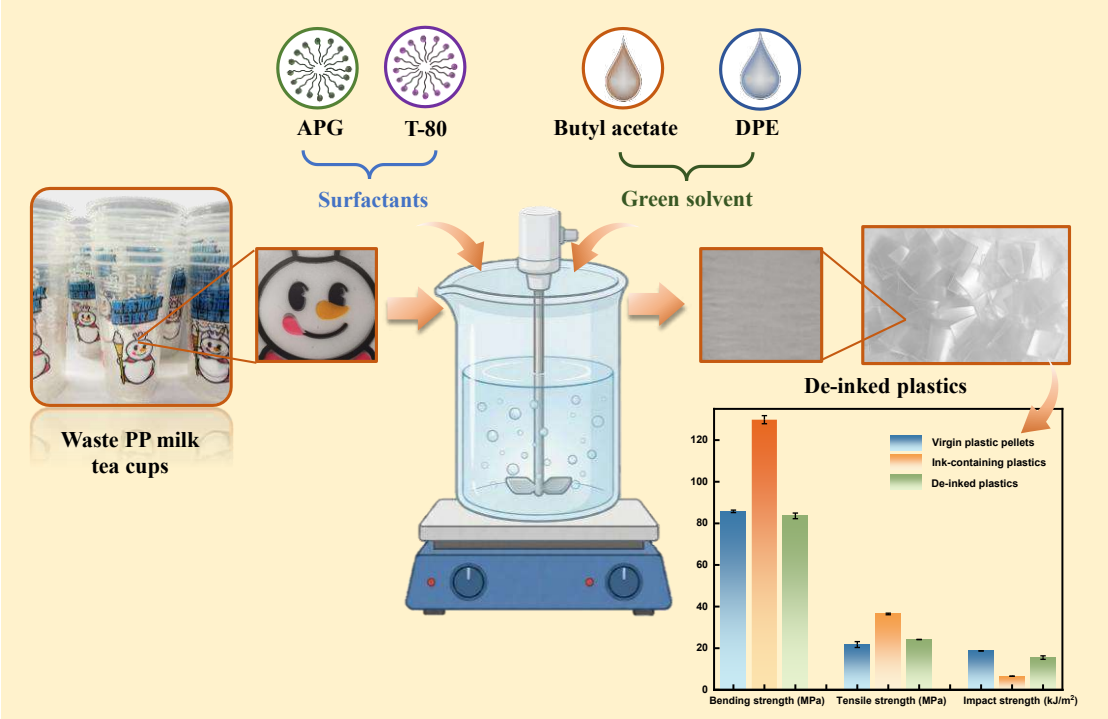
Lijun Xu [a], Yue Ning [a], Jingwen Xu [a], Nuo Xu [a], Qing Huang[a], Li Zhang[a], Jianming Zhu[a], Wenyi Yuan [a,*]

[a]*School of Resources and Environmental Engineering, Shanghai Polytechnic University, No. 2360 Jinhai Road, Shanghai 201209, P.R. China*

The corresponding authors: Wenyi Yuan

*Email: wyyuan@sspu.edu.cn

Graphical Abstract



Highlights

- Alkyl polyglucoside (APG)/Tween-80 (T-80) as deinking agent developed for de-inking milk tea cups.
- A deinking efficiency of 93.45% can be achieved under the optimal conditions.
- The deinking process well preserved the structure and mechanical properties of PP.

Abstract: Printing ink on waste polypropylene (PP) milk tea cups severely hinders their high-value recycling. A novel aqueous deinking system was developed with alkyl polyglucoside (APG)/Tween-80 (T-80) as composite surfactants and an eco-friendly mixed solvent of butyl acetate and dipropylene glycol ethyl ether (DPE). Deinking parameters were optimized via single-factor experiments and Box–Behnken response surface methodology, achieving a deinking efficiency of 93.45% under the optimal conditions: 3 wt.% surfactant, 13 wt.% organic solvent, 48 °C and 56 min. XRD characterization confirmed the intact α-crystal structure of PP after deinking. Mechanical properties tests showed that the impact strength of deinked PP was significantly recovered, while the bending and tensile strengths were essentially restored to the level of virgin PP. The deinking process followed a synergistic mechanism of solvent penetration, resin swelling, competitive adsorption, roll-up and emulsification. The efficient, low-damage and eco-friendly deinking system provides a promising technical approach for the high-value recycling of printed waste PP, facilitating the development of a circular plastic economy.

Keywords: Deinking efficiency; Polypropylene; Nonionic surfactants; Milk tea cup.

1. Introduction

The exceptional mechanical strength, chemical stability, and cost competitiveness of plastics have rendered them an indispensable component in modern industry and daily life[1, 2]. However, with the rapid growth of global plastic production, the environmental risks posed by plastic waste have emerged as a critical challenge for sustainable development[3, 4]. Against the background of carbon neutrality and circular economy promotion, the closed-loop recycling of plastics represents not only an

effective strategy to alleviate environmental pollution but also a necessary pathway to achieve high-value resource utilization[5, 6]. Despite the continuous advancement of recycling technologies, the presence of surface printing ink on waste polypropylene (PP) plastic products, such as beverage cups and takeaway containers, remains a key obstacle to high-quality recycling[7]. Ink is a complex multicomponent system, mainly consisting of resin binders, pigments, solvents, and additives[8, 9]. During conventional melt recycling, residual ink can cause discoloration and odor emission, and significantly deteriorate the mechanical properties and thermal stability of recycled plastics, frequently leading to downcycling[7, 10]. In contrast, upcycling strategies that convert plastic waste into value-added functional products, such as pigments, coatings and porous carbon materials, provide a route to retain more of the material value of recycled plastics[11-13]. The current deinking processes mainly involve physical friction, high-temperature pyrolysis, and chemical solvent washing[14]. Physical friction methods are largely ineffective in removing UV-cured inks due to their crosslinked structure[15]. High-temperature pyrolysis is energy-intensive and can degrade the polymer matrix. Conventional chemical deinking techniques, although relatively effective, typically utilize unsafe organic solvents such as halogenated hydrocarbons or caustic alkalis, which pose significant hazards in terms of volatile organic compound emissions and wastewater treatment[16, 17]. Therefore, the development of efficient deinking technologies is critical to enhancing the quality of recycled plastics and broadening their practical applications.

Currently, deinking agents are generally classified into four primary categories: organic solvent-based, semi-aqueous, aqueous, and lipase-based systems. Traditional organic solvent-based deinking methods remove ink primarily by dissolving the resin binders in solvents with similar chemical properties, which generate volatile organic compound emissions and associated wastewater treatment that impose significant environmental and safety risks[18]. Semi-aqueous and aqueous deinking systems rely on surfactants as the primary cleaning agents, attracting increasing attention due to their lower environmental impact and operational safety[19, 20]. Surfactants possess an amphiphilic structure, consisting of a hydrophilic head and a hydrophobic tail, which enables them

to significantly reduce interfacial tension at low concentrations, thereby facilitating the wetting, emulsification, and dispersion of ink components[21]. The same interfacial mechanisms also govern the surfactant-assisted separation of oily foulants from solid surfaces[22]. However, most current deinking agents still have three primary limitations: difficulty in penetrating complex cross-linked ink layers, insufficient adaptability to diverse ink chemistries, and inadequate understanding of the multi-component synergistic mechanisms required for efficient ink removal. These limitations often lead to incomplete ink removal or require harsh auxiliary conditions.

To address the above challenges, the study developed a novel aqueous deinking system composed of alkyl polyglucoside (APG) and Tween-80 (T-80) surfactant blends, coupled with a green mixed solvent of butyl acetate and dipropylene glycol ethyl ether (DPE). The system integrates the superior wetting ability of bio-based surfactants and the swelling effect of eco-friendly solvents to achieve efficient removal of complex ink layers. The deinking conditions were systematically optimized using single-factor experiments and response surface methodology. The influences of the deinking process on the physical properties of plastic substrates were evaluated, and the reusability of the deinking solution was also explored. Notably, the work provides an in-depth investigation into the multi-component synergistic mechanism, offering important theoretical support and technical guidance for the development of efficient and low-damage plastic recycling.

2. Preparation and Experimental Plan Design

2.1 Materials

The PP plastic used in the study was obtained from waste milk tea cups collected from a Mixue Ice Cream & Tea store. Uniform square samples of 22 mm × 22 mm were cut from plastic cups with the same surface printing for single-factor experiments and response surface methodology analysis. Crushed plastic fragments were used in the recycling tests of the deinking solution. All samples were rinsed with tap water to remove surface impurities and then dried at room temperature prior to use. To reduce experimental errors, samples with consistent patterns and colors were chosen for all

experiments.

Other reagents are listed in Table S1. All chemicals were of analytical grade or higher, and deionized water was used throughout the experiment. To ensure experimental accuracy, each test was performed at least in triplicate, and the average values were reported.

2.2 Experimental procedure

2.2.1 Deinking Experiment

The cut PP plastic specimens with colored printing ink were placed into a stainless-steel beaker, which was then filled with 100 mL of 15 wt.% deinking agent solution. In the study, the deinking agent was prepared via a strict sequential protocol to ensure complete mixing of the organic solvent phase with the aqueous phase and a homogeneous deinking bath. Specifically, a portion of deionized water was mixed with APG under continuous stirring. DPE was then slowly added to the mixture. Subsequently, a pre-blended solution of butyl acetate and T-80 was added dropwise under constant agitation. Finally, the remaining deionized water was used to rinse the container walls and adjust the final volume, thus completing the deinking agent formulation. The deinking treatment was conducted at 50 °C with continuous stirring using an electric stirrer for 45 min. After the treatment, the PP plastic pieces were retrieved, thoroughly rinsed with deionized water to remove surface residues, dried in a vacuum drying oven, and then stored for subsequent characterization and analysis.

2.2.2 Experiment on the Preparation of Test Specimens

A schematic diagram illustrating the preparation procedure of test specimens from recycled PP is presented in Figure S1. Firstly, the collected waste PP beverage cups were shredded using a large-scale shredder. The resulting fragments were rinsed with water and then dried. A small-scale granulator was used to further reduce particle size and obtain homogeneous plastic flakes. The obtained flakes were then melt-extruded using a plastic extruder. The extruded strands were pelletized with a pelletizer, and the resulting pellets were washed and dried again. Finally, standard test specimens were fabricated via injection molding using the as-prepared pellets.

2.2.3 Deinking Agent Circulation Test

Waste plastic cups were first fragmented using a high-speed crusher. Approximately 10 g of the obtained plastic fragments were weighed and transferred into a stainless-steel beaker. Subsequently, 200 mL of 15 wt.% aqueous deinking solution was added to the beaker. The deinking process was conducted at 48 °C with continuous stirring for 56 min using an electric stirrer. After the treatment, the plastic fragments were collected, thoroughly rinsed with deionized water to eliminate surface residual deinking solution, dried in a thermostatic oven, and stored for further characterization and analysis. The used deinking solution was preserved for the next cycle experiment. If excessive foaming appears in the deinking solution after each cycle, a small amount of industrial antifoaming agent can be added to eliminate the foam in a timely manner.

2.3 Test Method and Analytical Method

2.3.1 Image analysis and deinking efficiency calculation

To ensure the comparability of different samples, the residual area ratio was adopted as a quantitative index for the evaluation of ink residues in the study. The PP plastic specimens were scanned using the CamScanner application placed on a white card. The deinking efficiency was analyzed based on image processing via the OpenCV library (Python 3.11)[23], as described in the supplementary information. Considering the coexistence of multiple ink colors in the experimental specimens, independent identification protocols were established for each color category. The scanned images were first converted to the HSV (Hue-Saturation-Value) color space. Red and yellow ink residues were identified by color threshold segmentation combined with contour area filtering, while black ink residues were detected using a combined threshold of brightness and saturation, followed by morphological opening operations and geometric feature screening.

The deinking efficiency was defined as the degree of ink removal relative to the original non-deinked state and was shown in Equation 1:

$$\text{Deinking efficiency}\ (\%) = \frac{R_{max}-R_{sample}}{R_{max}-R_{min}} \times 100\% \quad (1)$$

In which, R_{max}, R_{min}, and R_{sample} denote the total residual area ratios of the original

non-deinked image, the fully deinked reference image (R_{min} = 0), and the tested sample image, respectively. The formula normalizes the deinking performance to a 0–100% scale, allowing quantitative and standardized evaluation of deinking efficiency. A typical visualization of the deinking efficiency calculation process obtained via Python is displayed in Figure 1. Further examples of deinked plastic samples and corresponding efficiency calculations are shown in Figure S2.

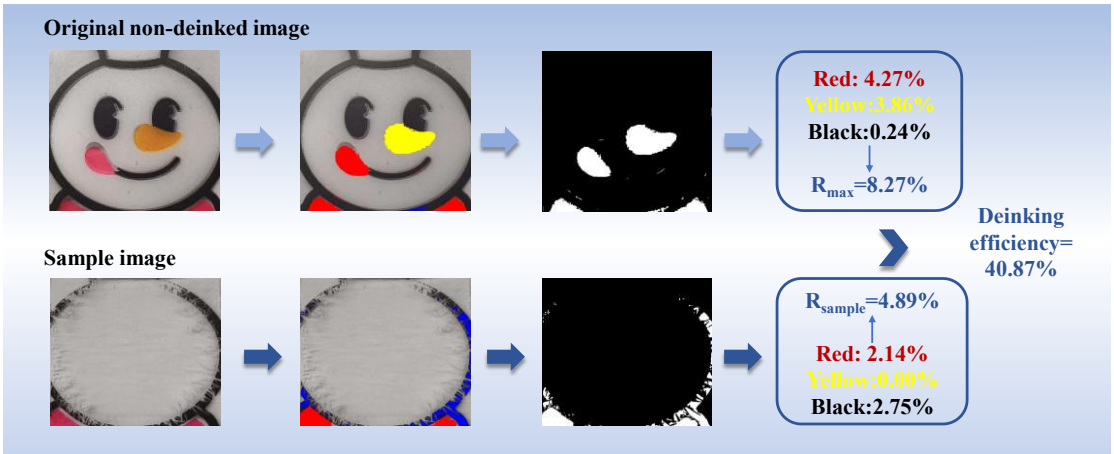


Figure1 Schematic of ink residue identification and deinking efficiency calculation via OpenCV in Python

2.3.2 Fourier Transform Infrared Spectroscopy (FTIR) Analysis

Fourier transform infrared (FTIR) spectroscopy (Thermo Fisher Nicolet iS20) was used to characterize ink residues on the surface of waste PP plastic. All tests were performed at 25 °C, with spectra recorded in the wavenumber range of 500–4000 cm^{-1} and 32 cumulative scans.

2.3.3 Performance Characterization of Surfactants

The foaming properties of the surfactants were investigated using a stirring method[24]. Specifically, the foaming behavior was examined at room temperature using an electric stirrer. For each measurement, 100 g of the prepared surfactant solution was transferred into a stainless-steel beaker and stirred at high speed for 60 s. Immediately after stirring, the mixture containing foam and liquid was transferred into a 500 mL graduated cylinder. The total foam volume was recorded, and the foam height was measured at 0 min (initial time) and after standing for 20 min. All experiments were performed in triplicate, and the average values of valid data were adopted as the final

results.

The emulsifying properties of the surfactants were evaluated using a shaking method. In each test, the surfactant solution and crude oil were mixed at a 1:1 volume ratio in a 20 mL stoppered test tube. The tube was sealed and placed in a constant-temperature water bath at 50 °C. The test tube was vigorously shaken several times at 5 min intervals to fully emulsify the oil-water mixture. After shaking, the tube was placed vertically in the water bath. The time required for the separation of 5 mL aqueous phase was recorded as the emulsification time. A longer emulsification time corresponds to stronger emulsifying performance. The average value of three parallel tests was used as the emulsification time at the corresponding concentration.

2.3.4 Biological microscopy characterization

To observe the morphological changes of ink residues before and after deinking treatment, plastic flakes from the original and deinked samples were separately mounted onto glass slides. Microscopic imaging was conducted at 40× magnification using a biological microscope (XSP-2CA).

2.3.5 Scanning Electron Microscope (SEM) test

To reveal the influence of the deinking process on the mechanical properties of recycled plastics, impact-fractured specimens were prepared using a pendulum impact tester. The fracture surfaces were characterized and analyzed using a scanning electron microscope (SEM, Hitachi S-4800).

2.3.6 X-ray Diffraction (XRD) Analysis

To investigate the effects of deinking and melt processing on the microstructure of polypropylene (PP) plastics, X-ray diffraction (XRD) analysis (Empyrean, PANalytical B.V.) was utilized. The scanning angle (2θ) ranged from 5° to 40° at a scanning speed of 2° min^{-1}. A Cu target X-ray tube was used as the radiation source, with an operating voltage of 40 kV and a current of 30 mA.

2.3.7 Mechanical Properties Testing of PP Plastic

To evaluate the mechanical properties of PP plastic before and after deinking treatment, a series of standard tests was performed in the study. All data are presented

as the average values obtained from five parallel specimens for each group. Flexural strength was measured in accordance with ASTM D790 using an electronic universal testing machine (Instron 3360, USA). The flexural strength was determined as the flexural stress at the maximum bending load. The specimen dimensions were 126.5 mm (length) × 12.64 mm (width) × 3.28 mm (thickness), with a test speed of 2 mm min^{-1}. Tensile testing was carried out on the same universal testing machine following ASTM D638. Tensile strength was defined as the yield stress, corresponding to the point at which the slope of the stress–strain curve equals zero. The dumbbell-shaped specimens had a total length of 165 mm, a parallel section width of 12.87 mm, a thickness of 3.28 mm, and an end width of 18.87 mm, with a test speed of 10 mm/min. Notched impact strength was tested according to ASTM D256 using a pendulum impact tester (Meters Industrial Systems (China) Co., Ltd., Model ZBC7000). The corresponding specimen dimensions were 63.5 mm (length) × 12.60 mm (width) × 3.28 mm (thickness).

3. Results and Discussion

3.1 Selection of primary components for deinking agents

In preliminary screening tests, the deinking efficiency of several common industrial cleaning surfactants was compared, as illustrated in Figure 2a. It was found that single-component surfactant solutions generally showed low overall deinking efficiency owing to insufficient penetration and dissolution ability toward ink resins. Among these surfactants, APG and T-80 exhibited relatively better deinking performance. As a high-performance bio-based nonionic surfactant, APG possesses ultra-low interfacial tension and excellent wettability[25], which can effectively promote the contact between solvents and the substrate interface. Meanwhile, T-80 possesses long polyoxyethylene chains that afford considerable steric hindrance[26], thereby favoring the long-term stable dispersion of detached ink fragments. Accordingly, APG and T-80 were chosen as key components of the composite system in the work, aiming to achieve efficient ink detachment and encapsulation under mild conditions through their synergistic effect. The foamability and emulsifying properties of APG/T-80 blends at different mass ratios were further investigated, as depicted in Figure 2b and Figure 2c. The results revealed

that a weight ratio of APG to T-80 of 4:1 led to a significant synergistic improvement in both properties. At the molecular level, the phenomenon can be attributed to the intermolecular interactions between the glucoside headgroups of APG and the polyoxyethylene chains of T-80. Such a synergistic assembly elevates the viscosity and elasticity of the interfacial film, thereby strengthening the mechanical strength and stability of the foam. Although the foam volume decreased markedly after 20 min, the relatively persistent stability indicates that the composite interfacial structure exhibits a certain resistance to external perturbations. Meanwhile, the emulsion stabilized by the 4:1 blend also demonstrated optimal performance. The enhancement is mainly ascribed to the synergistic adsorption and ordered arrangement of APG and T-80 at the oil-water interface. The hydrophobic moieties of the two surfactants can form a compact interfacial layer, which effectively reduces the interfacial tension and improves the kinetic stability of the emulsion. Overall, the 4:1 weight ratio maximized the ordered molecular arrangement and intermolecular interactions at the interface, enabling the surfactant composite system to achieve the best combination of foaming and emulsifying performance. It should be emphasised that the foaming behaviour is not merely an auxiliary indicator here, because the deinking bath is a vigorously stirred system in which the surfactant inevitably accumulates at the gas-liquid interface. Excessive and persistent foam is detrimental to deinking: it entraps the detached ink fragments and carries them into the foam layer, from which they may re-deposit onto the cleaned plastic during rinsing, and it also encloses the plastic fragments and thereby hinders their rinsing and recovery. In practice a small amount of an industrial antifoaming agent has to be added once excessive foaming appears in the recycled bath (Section 2.2.3). The APG/T-80 4:1 blend provides the combination required here, namely a high initial foam volume that reflects strong interfacial activity, together with a marked decay of the foam after 20 min standing, indicating that the foam is transient rather than persistent in the working bath.

The deinking efficiency of various organic solvents is showed in Figure 2d. According to their functional roles, these solvents were classified into penetrants and cosolvents. Butyl acetate, isophorone (IP), and *N*-methyl-2-pyrrolidone (NMP) were

selected as the main penetrants, which can dissolve the resin binder and promote ink detachment. Dipropylene glycol ethyl ether (DPE), diethylene glycol diethyl ether (DEGDEE), and dipropylene glycol methyl ether (DPM) were used as cosolvents. They help form a uniform and stable emulsion system with the aqueous surfactant phase[27] and prolong the effective contact time by slowing down the evaporation of the solvent system. Both butyl acetate and IP exhibited favorable deinking performance. However, IP was excluded from further investigation due to its higher cost and poorer environmental compatibility compared with other high-boiling-point solvents. NMP was not employed either, despite its strong dissolving capacity, because of its high biological toxicity and low biodegradability[28]. Among the cosolvents, DPE was chosen for its wide application as an additive in surfactants, paints, inks and coatings, as well as its use as an intermediate in the synthesis of resins, cellulose esters and other organic compounds. The deinking efficiency of plastic samples using butyl acetate and DPE at different blending ratios is displayed in Figure 2e. These results indicated that at a low DPE cosolvent ratio, butyl acetate disperses as large droplets in the aqueous phase owing to its poor water solubility. Although butyl acetate exhibits high solubility toward ink resins, it cannot be efficiently transported to the PP–ink interface via surfactant micelles. At a butyl acetate-to-DPE mass ratio of 3:2, DPE played a crucial role in micro-emulsifying butyl acetate and releasing it gradually into the deep regions of the ink layer. Meanwhile, butyl acetate provided sufficient solubilization to disrupt the intermolecular interactions within the resin. The synergistic effect of the two solvents contributes to the optimal deinking efficiency. In contrast, when the proportion of DPE was excessively high, the wettability and permeability of the system were further improved, but the inherently low deinking activity of DPE alone was insufficient to break the intermolecular linkages of the resin. Even with sufficient contact between the solvent and the ink, efficient ink detachment remained difficult to achieve. Consequently, the deinking efficiency decreased continuously as the butyl acetate ratio declines.

FTIR spectra of the ink layer delaminated from the PP plastic surface are shown in Figure 2f. The absorption peak at 1719.2 cm^{-1} was assigned to the stretching vibration

of the C=O bond, while the peaks at 1259.3 cm^{-1} and 1165.3 cm^{-1} correspond to the asymmetric and symmetric stretching vibrations of the C-O-C linkage in ester groups, respectively. The strong absorption band at 2913.9 cm^{-1} was attributed to the C-H stretching vibrations of alkyl groups. These characteristic peaks were indicative of an acrylic resin-based system. In addition, no absorption bands were detected in the wavenumber range of 3300-3400 cm^{-1}, which rules out the presence of polyurethane or polyamide binders. Combined with the spectroscopic evidence and the rapid dissolution behavior of the ink in ester solvents such as butyl acetate, it can be concluded that the primary resin binder in the ink formulation is an acrylic polymer[29].

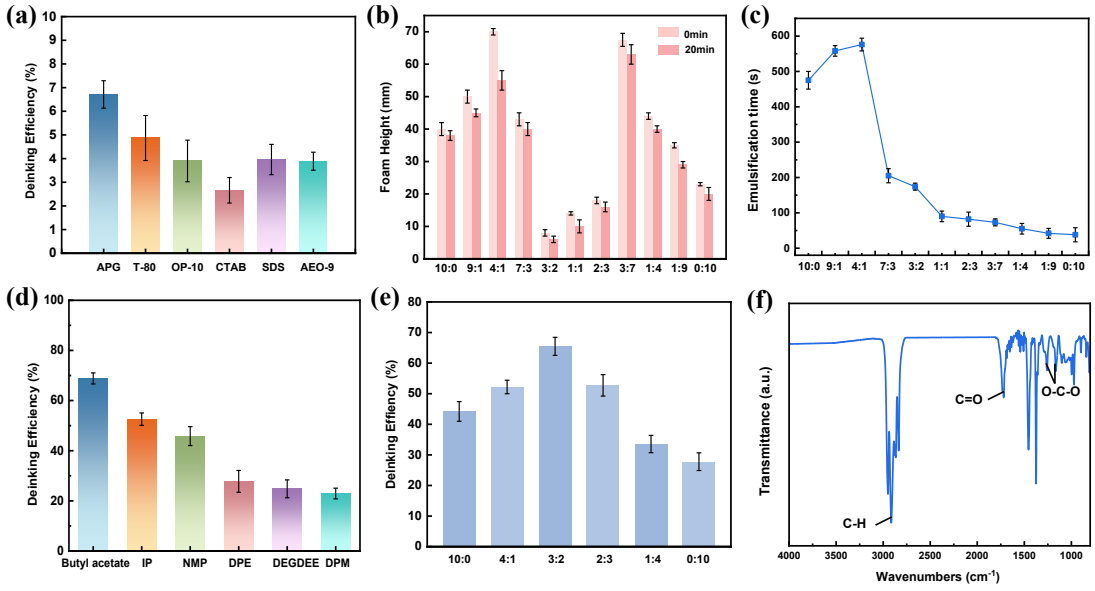


Figure 2 (a) Deinking efficiency of different industrial surfactants; (b) the foamability performance of blended systems containing APG and T-80 at varying mass ratios; (c) the emulsifying performance of blended systems containing APG and T-80 at varying mass ratios; (d) the deinking efficiency of different organic solvents; (e) the deinking performance of plastic samples treated with varying blend ratios of butyl acetate and DPE; (f) FTIR spectra of ink layers peeled from PP plastic surfaces.

3.2 Single factor experiments of the preparation of deinking agents

As illustrated in Figure 3a, the deinking efficiency reached a maximum at an optimal surfactant concentration, and decreased gradually at higher concentrations. Within the low concentration range of 1 wt.% to 3 wt.%, the adsorption of surfactant at

relevant interfaces was not yet saturated. Increasing the surfactant concentration substantially reduced the interfacial tension and enhanced wettability[30], facilitating the emulsification of detached ink fragments and inhibiting their redeposition. Consequently, the deinking efficiency was found to increase sharply with increasing surfactant concentration. At 5 wt.%, interfacial adsorption approached saturation, and an optimal balance between emulsification and penetrability is achieved, yielding the maximum deinking efficiency. However, when the concentration was further increased to 7-9 wt.%, the deinking efficiency plateaus, which was mainly attributed to micellar solubilization [31]. Under these conditions, excess surfactant molecules aggregated into high-density micelles that solubilize the organic solvent. thereby reducing its effective concentration available for interacting with the ink-substrate interface. Moreover, the enhanced foaming tendency at elevated concentrations suggested that surplus surfactant preferentially accumulated at the gas-liquid interface rather than contributing to the deinking process[32]. Therefore, 5 wt.% was identified as the optimal concentration that balances deinking performance with reagent economy.

As illustrated in Figure 3b, the deinking efficiency exhibits an initial rapid increase with rising total organic solvent concentration, followed by a decline beyond a critical threshold. In the low-concentration regime, the deinking performance is constrained by insufficient dissolution kinetics. At these levels, the solvent molecules exhibited a low chemical potential, while the resin matrix maintained a high degree of cross-linking and physical chain entanglement. Consequently, the solvent only induced superficial wetting of the resin surface and fails to induce adequate relaxation of the polymer within the deeper layers of the ink film. The results in the ink layer remaining tenaciously bonded to the PP substrate. Upon reaching a concentration of 10 wt.%, the system attained an optimal dynamic equilibrium between solvent penetration and polymer dissolution. The synergistic combination of butyl acetate and DPE provided sufficient solvating power to rapidly permeate the ink layer and induce significant resin swelling[33]. At the critical concentration, the chemical action of the solvents coincided with the interfacial disjoining pressure generated by the surfactants[34], facilitating efficient ink detachment while limiting solvent penetration into the amorphous regions

of PP to a slight and reversible level. However, above the concentration of 10 wt.%, the deinking efficiency reached a plateau, followed by a decrease. Excess solvent molecules gradually acted on the plastic substrate, inducing significant polymer chain disentanglement and a pronounced plasticizing effect[35]. The excessive swelling disrupted the intermolecular forces within the PP matrix, macroscopically manifested as substrate softening, surface tackiness, and a loss of mechanical strength. Therefore, 10 wt.% represented not only the peak deinking efficiency but also a critical process threshold that balances cleaning efficacy with substrate compatibility.

As shown in Figure 3c, the deinking efficiency initially increased with rising temperature and declined with further temperature elevation. In the low temperature range of 30-50 °C, the temperature increase provided thermal kinetic energy to solvent molecules such as butyl acetate and DPE, thereby accelerating their penetration into and swelling of the acrylic resin matrix. This treatment effectively reduced the interfacial adhesion energy between the ink layer and the PP substrate. At 50 °C, the system achieved an optimal synergistic state, in which the solvency power of the organic solvents and the competitive adsorption kinetics of the surfactants were balanced. This balance supplied sufficient energy to overcome the desorption energy barrier and maximized the deinking efficiency. However, when the temperature was further raised to 60 °C and above, the deinking efficiency either plateaued or showed an obvious decrease. This deterioration was mainly attributed to the negative side effects caused by excessively high temperatures. On the one hand, the evaporation rate of the organic solvents rose sharply, which lowered the concentration of active components in the liquid phase and weakened the chemical attack on the interfacial ink layer. On the other hand, the high temperature approached the heat deflection temperature of the PP substrate and enhanced the mobility of polymer chains. This shifted the main function of the solvent from interfacial ink detachment to penetration into the substrate, leading to significant macroscopic swelling, softening, and permanent deformation of the PP sheets. Therefore, the highest deinking efficiency was achieved at 50 °C, which also corresponded to a critical processing threshold ensuring a favorable balance between deinking performance and the physical integrity of the PP

substrate.

As presented in Figure 3d, the deinking efficiency exhibited a rapid initial increase with extended treatment time, followed by a gradual approach to a plateau. In the early stage, the process was predominantly governed by external mass transfer. The vigorous shear forces generated by mechanical agitation substantially reduced the thickness of the diffusion boundary layer at the solid-liquid interface. The reduction accelerated the transport of fresh deinking agents to the ink surface and enhanced solvent penetration into, and subsequent swelling of, the acrylic resin matrix, thereby facilitating the detachment of the ink layer from the plastic substrate. After approximately 45 min, the efficiency curve began to level off, indicating a shift in the rate-limiting step from external mass transfer to internal diffusion control. Prolonging the treatment time beyond the point yielded marginal gained in deinking efficiency while incurring non-productive energy consumption. Therefore, based on both process efficacy and economic considerations, a treatment duration of 45 min was identified as optimal for the system.

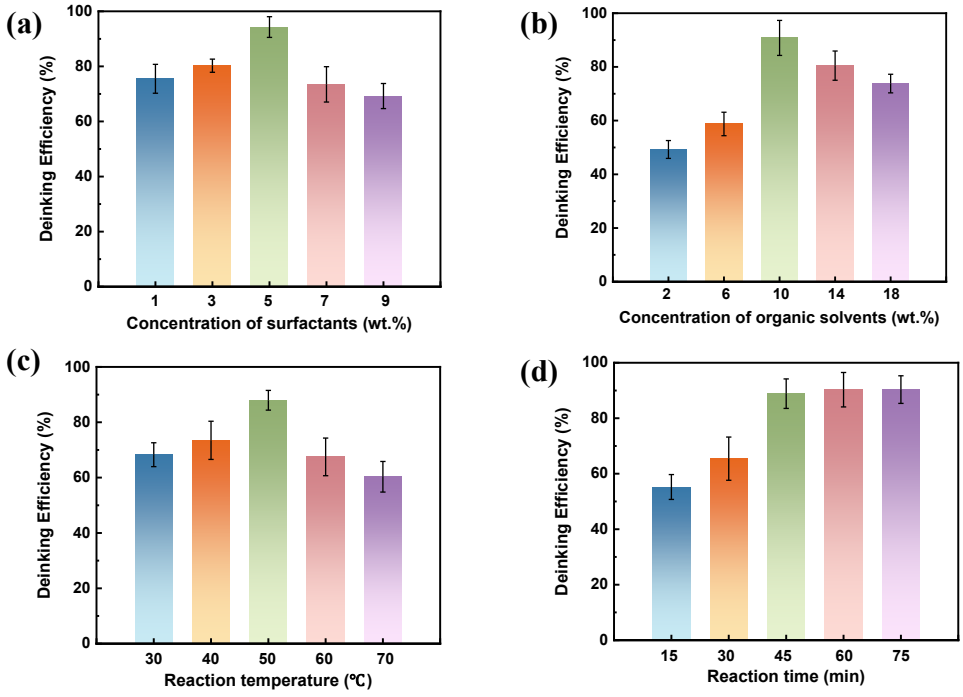


Figure 3 (a) Effect of surfactant concentration on deinking efficiency; (b) Effect of organic solvent concentration on deinking efficiency; (c) Effect of treatment temperature on deinking efficiency; (d) Effect of treatment time on deinking efficiency.

3.3 Response surface analysis of the preparation of deinking agents

Based on the results of single-factor experiments, surfactant concentration, organic solvent concentration, temperature, and treatment time were selected as independent variables, with deinking efficiency as the response variable. A total of 29 experimental runs, including five replicates at the center point, were conducted, and the corresponding results are presented in Table S2. The data indicate that deinking efficiency across different conditions ranged from 29.12% to 97.6%, demonstrating that the selected factors induced substantial variation in the response. The variability provides a robust foundation for model construction and subsequent optimization.

Considering the analysis of the experimental data in Table S2 using Design-Expert 13 software yielded the following quadratic regression equation (Equation 2):

$$DE\ (\%) = 92.13-2.73A+14.01B-3.82C+2.98D-4.24AB-1.04AC-2.58AD-1.85BC+ 1.27BD-3.05CD-4.95A^2-24.7B^2-17.74C^2-6.89D^2 \quad (2)$$

As presented in Table S3, the regression model is highly significant ($P < 0.0001$). The lack of fit is insignificant ($P = 0.5116$), indicating that the model adequately fits the experimental data. The coefficient of determination ($R^2 = 0.9564$) demonstrates a strong correlation between the experimental and predicted values. Furthermore, the difference between the adjusted R^2 ($R^2_{Adj} = 0.9127$) and the predicted R^2 ($R^2_{Pred} = 0.7980$) is less than 0.2, confirming the model's predictive capability, reliability, and conformance to the precision requirements of response surface methodology. Table S3 summarizes the analysis of variance (ANOVA) results obtained from the Box-Behnken design (BBD). The ANOVA reveals that the concentrations of organic solvents (B) and treatment temperature (C) have statistically significant effects on deinking efficiency ($P < 0.05$), whereas surfactant concentration (A) and treatment time (D) do not exhibit significant effects ($P > 0.05$). All quadratic terms (A^2, B^2, C^2, and D^2) are significant ($P < 0.05$). The relative influence of the factors on deinking efficiency follows the order: concentration of organic solvents (B) > treatment temperature (C) > treatment time (D) > concentration of surfactants (A). The validity of the regression model is attributed to the appropriate selection of factor levels, which effectively span the critical response

region of deinking efficiency. The optimal process parameters identified through response surface optimization lie within the design space. The combined significant model fit and non-significant lack-of-fit confirm that the chosen factor levels encompass the region containing the optimal extreme values.

As shown in Figure 4 and Figure S3, the response surface and contour plots illustrate the interactive effects of the selected factors on deinking efficiency. The results indicate that the interaction between the concentration of surfactants (A) and the concentration of organic solvents (B) exerts a pronounced influence on deinking efficiency, as evidenced by the marked curvature of the corresponding response surface. The interaction terms, ranked in ascending order of their effects on deinking efficiency, are AB > CD > AD > BC > BD > AC, which is consistent with the analysis of variance results presented in Table S3. Regarding the observed trends, deinking efficiency initially increases and then decreases with increasing concentrations of surfactants (A) and organic solvents (B).

Based on the response surface regression model, the predicted optimal process parameters for plastic deinking were determined as follows: surfactant concentration 3 wt.%, organic solvent concentration 13 wt.%, treatment temperature 48 °C, and treatment time 56 min, with a corresponding predicted deinking efficiency of 96.05%. Experimental verification under these conditions yielded a deinking efficiency of 93.45±3.85%, which closely aligns with the predicted value, thereby confirming the reliability of the model.

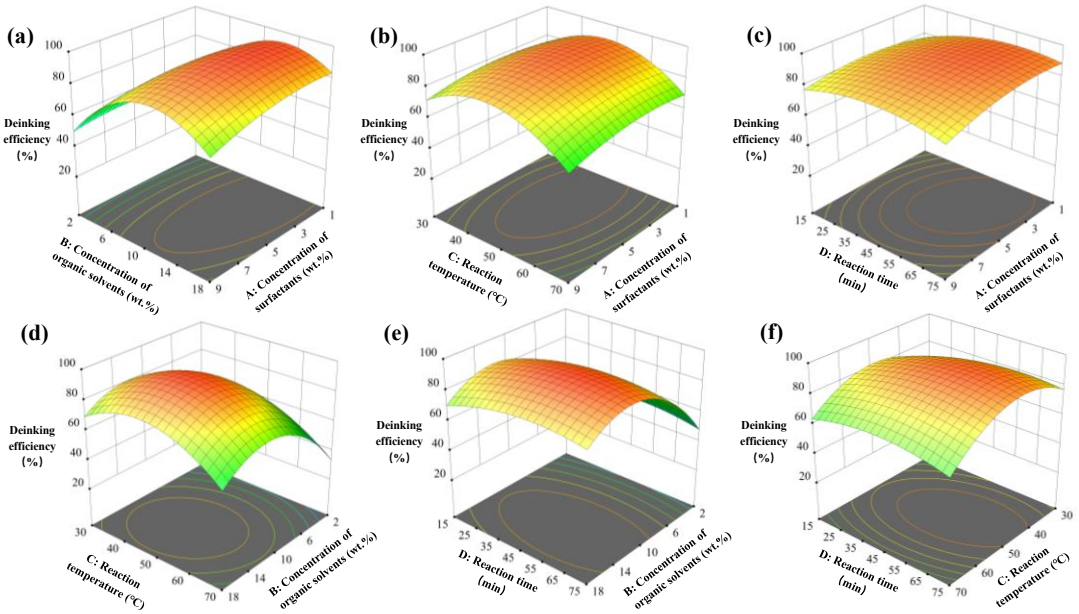


Figure 4 Surface plots for the effect of interaction factors on deinking efficiency. (a) Concentration of organic solvents and concentration of surfactants; (b) Treatment temperature and concentration of surfactants; (c) Treatment time and concentration of surfactants; (d) Treatment temperature and concentration of organic solvents; (e) Treatment time and concentration of organic solvents; (f) Treatment time and treatment temperature.

3.4 The effect of ink on the appearance and physical properties of plastics

The selected plastic samples were surface-printed with colored ink and cut into appropriate dimensions for the deinking experiments. Optical images of these samples, showing their appearance before and after treatment with the deinking agent, are presented in the corresponding figure. As can be observed from Figure 5, the ink coverage area differs markedly before and after the treatment process. Following treatment, the surface ink is almost completely removed, achieving a high overall degree of elimination. The result demonstrates that the deinking agent developed in the study exhibits effective deinking performance.

During the plastic deinking process, using a biological microscope enables clearer discrimination between the ink and the plastic substrate interface. Figure 6a-6c present the microstructural characterization of plastic before deinking, during the deinking process, and plastic after deinking. As evidenced by the micrographs, the condition of the ink on the plastic surface underwent remarkable changes over time. Before the

deinking, a distinct color contrast existed between the ink and the plastic surface, with a clearly discernible boundary. During the deinking process, the ink-covered area progressively diminished as the treatment proceeds. After the deinking, the ink was observed to be almost completely removed, indicating that the ink molecules on the plastic substrate surface had been largely detached. To elucidate the relationship between macroscopic mechanical properties and microstructural characteristics, scanning electron microscopy (SEM) was employed to examine the cross-sections of virgin PP pellets, ink-containing PP plastics, and de-inked PP injection-molded specimens, as presented in Figure 6 (d-f) and Figure S4. The cross-sectional morphology of the virgin PP specimen (Figure S4-a) is depicted in Figure 6d, revealing a homogeneous, dense, and continuous matrix. Only minor micro-voids and molecular chain alignment traces resulting from the injection molding process were observable[36]. Figure 6e reveals a highly heterogeneous microstructure in the ink-containing PP sample (Figure S4-b)[37]. The ink system includes rigid particles of pigment such as TiO_2 and $CaCO_3$[38], which are dispersed at the micrometer scale within the PP skeleton. Although these rigid particles may enhance material strength through a skeleton-support effect, the distinct interfacial boundaries arising from poor compatibility between the particles and the matrix introduce interfacial defects. Figure 6f presents the cross-sectional morphology of the de-inked PP specimen (Figure S4-c), which closely resembles that of the virgin PP matrix. Only slight roughening is observable on the surface and within the matrix, attributable to minute pits formed during the deinking process. The SEM observations provided microscopic evidence elucidating the differences in macroscopic behavior of PP materials under various conditions. The incorporation of ink introduced heterogeneous defects within the matrix, thereby impairing the material's toughness. Conversely, the deinking process not only successfully removed the majority of ink components but also presented an opportunity to restore and potentially enhance the mechanical performance of the recycled material.

X-ray diffraction (XRD) analysis was conducted on virgin plastic pellets, ink-containing recycled plastic, and de-inked recycled plastic to systematically investigate the influence of processing and deinking on the material's microstructure. As shown in

Figure 7a, all samples exhibit prominent diffraction peaks at approximately 14.8°, 17.6° and 19.2°, corresponding to the (110), (040) and (130) crystallographic planes of PP, respectively[10]. The strong overlap of diffraction peaks among the three patterns indicates that neither the presence of ink nor the treatment with deinking agents modified the monoclinic α-crystal form of PP, thus verifying the structural stability of the material. Figure 7b and Table S4 show the comparison of the mechanical properties of virgin plastic pellets, ink-containing plastic and de-inked plastic. The bending strength of the ink-containing sample was 129.82±1.95 MPa, and its tensile strength was 34.65±0.38 MPa, both of which were markedly higher than those of the virgin PP (85.77±0.60 MPa and 21.79±1.42 MPa, respectively) (Table S4). This phenomenon could be attributed to the rigid inorganic pigment particles in the ink, which acted as a reinforcing phase in the polymer matrix and effectively restricted the slippage of molecular chains[39]. It should be emphasised that the waste cups were first crushed, subsequently pelletised and finally injection-moulded, so that the ink layer originally confined to the cup surface was fragmented and homogeneously dispersed throughout the bulk of the specimen rather than remaining as a surface coating; the reinforcing effect of the rigid pigment particles therefore operates on the entire matrix, which is consistent with the uniform darkening observed in the injection-moulded specimens (Figure S4-b). However, the interfaces between these rigid particles and the matrix introduced structural defects and severe stress concentration in the ink-containing plastics, resulting in a pronounced decrease in impact strength to 6.54±0.03 kJ/m² (Table S4). After deinking, the bending strength (83.58±1.36 MPa) and tensile strength (24.18±0.07 MPa) were restored to a level comparable with that of the virgin plastics, indicating that the treatment caused no measurable degradation of the PP matrix itself. Moreover, the impact strength of the deinked plastic (15.5 ± 0.83 kJ/m²) was significantly superior to that of the ink-containing plastic (6.54 ± 0.03 kJ/m²), corresponding to a recovery of more than 80% of the value measured for the virgin

plastic (18.73±0.07 kJ/m²). Since the mechanical performance of recycled PP is highly sensitive to its processing history, such lot-by-lot verification of mechanical properties is essential for the quality control of recycled plastics[40].



Figure 5 Optical images of plastic samples before and after deinking treatment

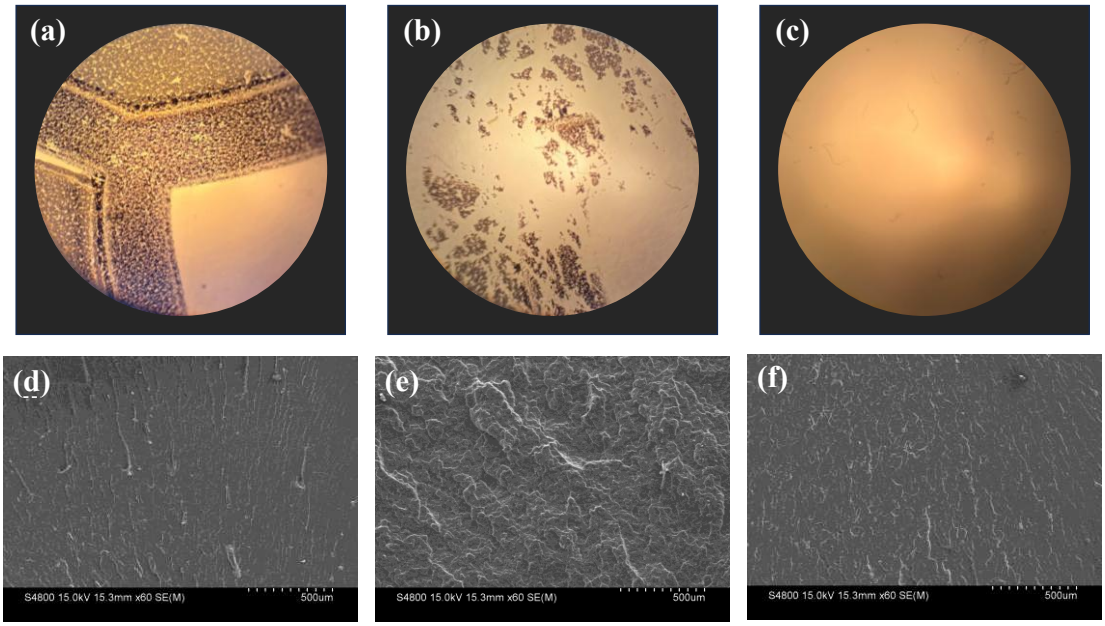


Figure 6 Biological microscope images of plastic samples. (a) plastic before deinking; (b) during the deinking process; (c) plastic after deinking. SEM image of a mechanical spline cross-section. (d) the virgin PP specimen; (e) the ink-containing PP specimen; (f) the deinked PP specimen.

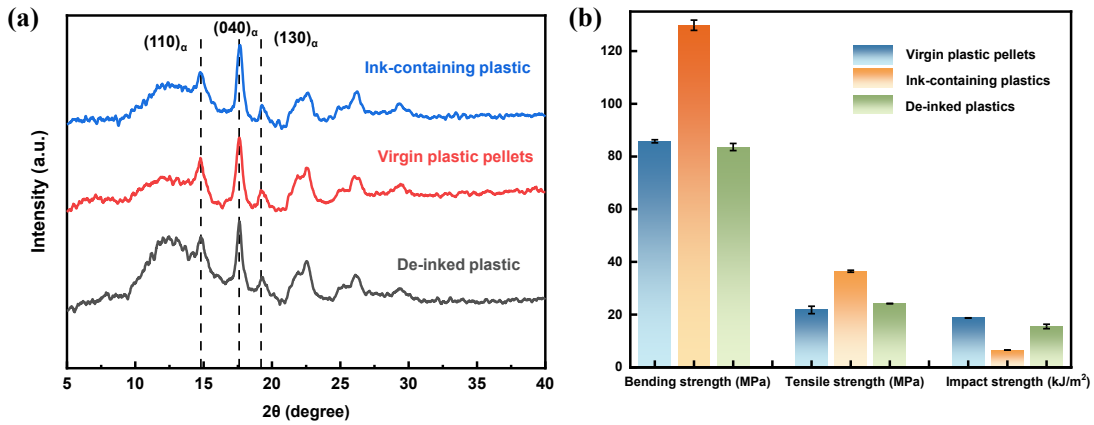


Figure 7 (a) XRD Characterization of plastic crystal structures under ink and deinking treatment; **(b)** The effect of ink on material physical properties.

3.5 Recycling of deinking agents

To assess the economic viability of deinking agent recycling, four consecutive cycle experiments were conducted. As illustrated in Figure 8, the deinking efficiency was substantially influenced by the number of cycles, decreasing from 92.98% in the first use to 24.1% by the fourth cycle. The performance decline results from the synergistic effects of multiple factors. On one hand, the organic solvent components within the deinking agent are progressively depleted throughout the recycling process. On the other hand, ink fragments, pigment particles, and dissolved resins retained in the recycling solution not only occupy active sites on surfactants and solvents but may also form a physical barrier at the interfaces, thereby hindering effective contact between fresh chemicals and the residual ink. Therefore, the type of formulation can be recycled to decrease the amount of virgin material and increase the efficiency in resource use.

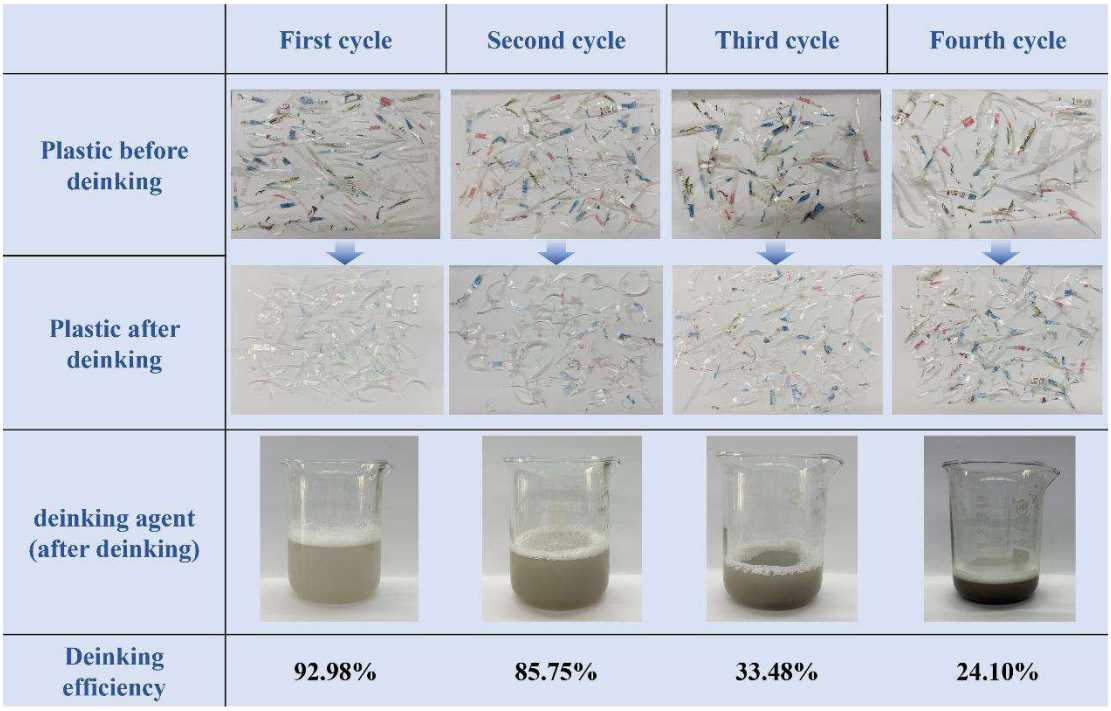


Figure 8 Deinking agent circulation experiment record chart

3.6 Analysis of the deinking mechanism

The deinking agent prepared in the study undergoes four sequential stages during the deinking process[21] (shown in Figure 9**)**.

Stage I: Initial Interfacial Adhesion (Figure 9a). Pigments are encapsulated in a crosslinked acrylic resin binder[41]. Owing to the industrial corona treatment applied to the PP surface, the interfacial adhesion between the ink and PP is mainly governed by van der Waals forces and localized interfacial hydrogen bonds. These hydrogen bonds are formed between functional groups such as carboxyl and hydroxyl groups in the acrylic resin and oxygen-containing active sites on the PP surface [42].

Stage II: Solvent Penetration and Competitive Adsorption (Figure 9b). When the deinking agent is added, butyl acetate and DPE rapidly penetrate the resin matrix. The introduction of organic solvents induces swelling and relaxation of resin molecular chains, increasing the intermolecular distance and thereby weakening the van der Waals forces. APG molecules then migrate to the ink-PP interface and anchor onto the freshly exposed PP surface through their hydrophobic alkyl chains via hydrophobic interaction, while their hydrophilic glucoside head groups remain oriented towards the aqueous phase. Because the non-polar PP surface interacts far more favourably with the alkyl

chains than with the polar resin segments that are hydrogen-bonded to it in Stage I, this competitive adsorption progressively displaces the original resin binder, and the interfacial hydrogen bonds established in Stage I are broken as the aqueous phase penetrates the interface, thus disrupting the interfacial integrity.

Stage III: Roll-up and Interfacial Separation (Figure 9c). Under the synergistic effect of APG and T-80, the interfacial tension decreases significantly, causing the ink layer to bend and gradually contract. Surfactant molecules rearrange, with their hydrophobic tails adsorbing onto the newly deinked PP surface, which inhibits the secondary adsorption of pigment particles on the PP substrate.

Stage IV: Emulsification and Dispersion (Figure 9d). The detached ink is fragmented under fluid shear forces, after which two distinct dispersion pathways operate simultaneously. Resin molecules and low-molecular-weight oligomers released from the swollen binder are solubilised within the mixed micelles formed by APG and T-80, i.e. they are incorporated at the molecular level into the hydrophobic core of the micelles. The much larger micron-scale ink fragments and pigment agglomerates, by contrast, are far too large to be accommodated inside nanometre-sized micelles; these are emulsified and dispersed as suspended particles in the aqueous phase, stabilised by the adsorbed surfactant layer. APG facilitates interfacial tension reduction to promote ink fragmentation, while T-80 plays a decisive role at this stage. With its high molecular weight and long polyethylene oxide chains, T-80 provides considerable steric hindrance, which prevents pigment particles from re-adsorbing onto the cleaned PP surface and ensures the high-purity recovery of plastic fragments.

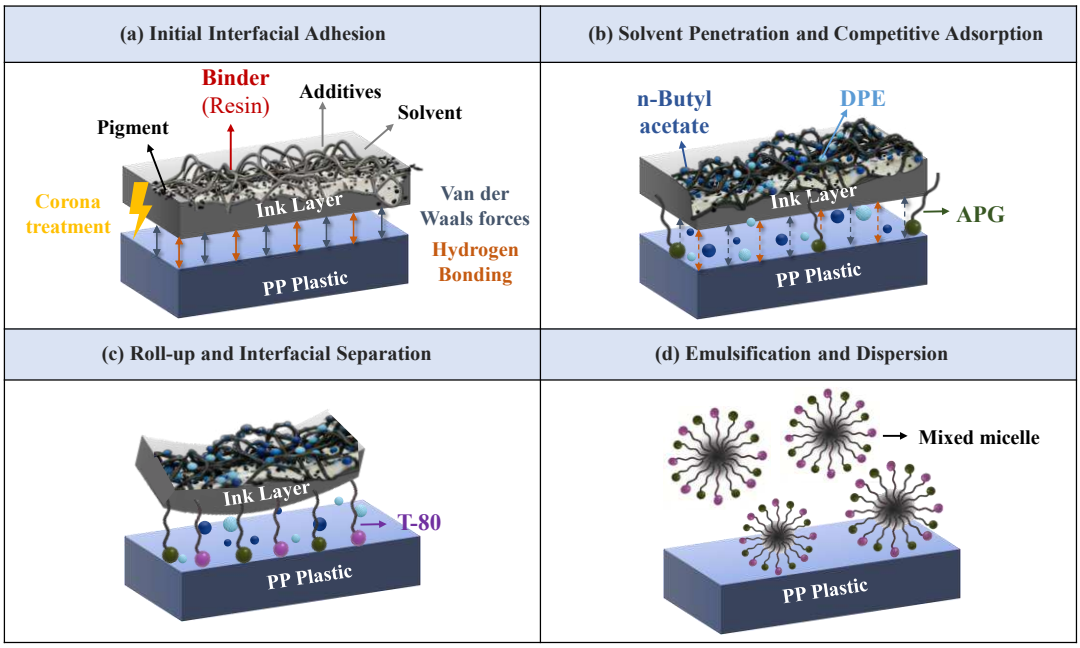


Figure 9 Deinking agent deinking mechanism diagram

4. Conclusion

In this research, a deinking agent was successfully developed using APG, T-80, butyl acetate, and DPE, which exhibits excellent performance in removing printing ink from waste PP. Single-factor experiments combined with response surface methodology were employed to optimize the deinking process parameters. Under the optimal conditions, using 3 wt.% surfactant, 13 wt.% organic solvent, a temperature of 48°C, and a treatment duration of 56 min, the deinking process yielded an efficiency of 93.45%. XRD characterization confirmed that the inherent crystalline structure of PP remained intact during the deinking process, without structural damage. Mechanical property tests demonstrated that the deinking treatment effectively restored the mechanical properties of waste PP. The bending and tensile strengths of the deinked plastic were comparable with those of the virgin PP, and the impact toughness recovered to more than 80% of the virgin value, which is attributed to the effective removal of the rigid pigment particles that otherwise act as stress concentrators in the matrix. Mechanistic analysis revealed that the high deinking efficiency was achieved through the synergistic effects of multiple steps, including solvent penetration, resin swelling, competitive adsorption, ink roll-up, and emulsification. Although repeated recycling

led to a slight decrease in deinking efficiency due to the loss of deinking components, the proposed deinking system still provides a viable, eco-friendly approach for the high-value recycling of waste PP, thereby contributing to the establishment of a circular plastic economy.

Acknowledgements

The authors greatly thank the financial support from National Natural Science Foundation of China (No. 22576131), Pudong Minsheng Program (PKJ2022-C02, PKJ2022-C06) and Natural Science Foundation of Shanghai (24ZR1425300).

References

[1] Brandon A, Vanapalli K R, V. Martin O, et al. Charting success for the plastics treaty. *One Earth*, **2023**, *6*, 575-581.
[2] Chin M T, Diao T. Industrial and laboratory technologies for the chemical recycling of plastic waste. *ACS Catalysis*, **2024**, *14*, 12437-12453.
[3] Cudjoe D, Wang H. Plasma gasification versus incineration of plastic waste: energy, economic and environmental analysis. *Fuel Processing Technology*, **2022**, *237*, 107470. 10.1016/j.fuproc.2022.107470.
[4] Kwon G, Cho D-W, Park J, et al. A review of plastic pollution and their treatment technology: A circular economy platform by thermochemical pathway. *Chemical Engineering Journal*, **2023**, *464*, 142771.
[5] Damayanti D, Saputri D R, Marpaung D S S, et al. Current prospects for plastic waste treatment. *Polymers*, **2022**, *14*, 3133.
[6] Li Y, Shan G, Hao S, et al. Systemic governance and circular economy synergies: a multidimensional analysis of China's "zero-waste cities" initiative. *Circular Economy*, **2025**, *4*, 100153.
[7] Ügdüler S, Van Laere T, De Somer T, et al. Understanding the complexity of deinking plastic waste: an assessment of the efficiency of different treatments to remove ink resins from printed plastic film. *Journal of Hazardous Materials*, **2023**, *452*, 131239.
[8] Lisiecki M, Bele T G A, Ugduler S, et al. Mechanical recycling of printed flexible plastic packaging: the role of binders and pigments. *Journal of Hazardous Materials*, **2024**, *472*, 134375.
[9] Sonmez S, Salam A, Fleming P D, et al. Usability of cellulose-based binder in water-based flexographic ink. *Coloration Technology*, **2023**, *139*, 239-247.
[10] Phanthong P, Miyoshi Y, Yao S. Development of tensile properties and crystalline conformation of recycled PP by re-extrusion using a twin-screw extruder with an additional molten resin reservoir unit. *Applied Sciences*, **2021**, *11*, 1707.
[11] Zhou X, Yang L, Shao Y, et al. Highly efficient depolymerization of waste polyethylene terephthalate for upcycling in colorful pigments and coatings. *Journal of Materials Science & Technology*, **2026**, *251*, 59-70.
[12] Fu D, Zhou X, Li D, et al. Functional upcycling waste polyethylene terephthalate plastics for high near-infrared reflective pigment via controlled molecular reconstruction. *Dyes and Pigments*, **2026**, *254*, 113973.
[13] Li D, Shao Y, Zhang J, et al. Upgrading waste polyethylene terephthalate with lignin into functional carbon materials with tunable pores for high-efficiency adsorption.

Sustainable Materials and Technologies, **2026**, *49*, e02167.
[14] Zhang Y G. Innovative drive of green cleaning solutions for recycled plastic resources from waste plastic packaging. *Plastic Packaging*, **2019**, *29*, 1-11.
[15] Yan W, Hou C. Preparation and properties of UV anti-corrosion ink. *Journal of Macromolecular Science Part A-Pure and Applied Chemistry*, **2025**, *62*, 95-103.
[16] Ye X, Wu Z, Wang M, et al. Effectively remove printing ink from plastic surface over quaternary ammonium-modified waste cooking oil. *Environmental Technology*, **2023**, *44(8)*, 1071-82.
[17] Syed Ali S A, Ilankoon I M S K, Zhang L, et al. Understanding de-inking in packaging plastic recycling: Bridging the gap in resource conservation and establishing average hazard quotient. *Journal of Hazardous Materials*, **2024**, *479*, 135554.
[18] Zhang Z, Wang M, Wang D, et al. Technological advances in solvents drive a significant decrease in VOC emissions and negative impacts from industrial solvent-use sources. *Environmental Pollution*, **2025**, *385*, 127046.
[19] Wang T, Chang D, Huang D, et al. Application of surfactants in papermaking industry and future development trend of green surfactants. *Applied Microbiology and Biotechnology*, **2021**, *105*, 7619-34.
[20] Kumar Shah S, Chakraborty G, Bhattarai A, et al. Synergistic and antagonistic effects in micellization of mixed surfactants. *Journal of Molecular Liquids*, **2022**, *368*, 120678.
[21] Guo J, Luo C, Wittkowski C, et al. Screening the impact of surfactants and reaction conditions on the de-inkability of different printing ink systems for plastic packaging. *Polymers*, **2023**, *15(9)*, 2220.
[22] Zhou X, Li D, Wang L, et al. Recent advances in the modification of melamine sponge for oil-water separation. *Journal of Materials Science & Technology*, **2025**, *207*, 209-224.
[23] Syed Ali S A, Ilankoon I M S K, Zhang L, et al. Response surface methodology optimisation of catanionic surfactant mixtures in de-inking packaging plastic waste. *Journal of Hazardous Materials*, **2025**, *499*: 140244.
[24] Ma J-W, Zhang Z-J, Li Y-Q, et al. Synthesis and properties of low-foaming nonionic gemini surfactants. *Acta Polymerica Sinica*, **2024**, *55*, 1356-1364.
[25] Zhang J, Ni X, Liu G, et al. Wetting behaviors and mechanisms of coal modified by different types of surfactants under intervention using KCL. *Langmuir*, **2025**, *41*, 10250-62. 10.1021/acs.langmuir.5c00074.
[26] Wang H, Lin X, Zhu J, et al. Encapsulation of lutein in gelatin type A/B-chitosan systems via tunable chains and bonds from tweens: thermal stability, rheologic property and food 2D/3D printability. *Food Research International*, **2023**, *173*: 113392. 10.1016/j.foodres.2023.113392.
[27] Zhang G, Peng H, Wei Q, et al. Improving the performance of si/pedot:pss hybrid solar cells with more economical and environmentally friendly alcohol ether solvents. *ACS Omega*, **2024**, *9*, 15040-51. 10.1021/acsomega.3c09187.
[28] Li N, Han X, Lv H, et al. Biodegradation of N-methyl-2-pyrrolidone (NMP) in wastewater: a review of current knowledge and future perspectives. *Journal of Cleaner Production*, **2025**, *486*: 144452. 10.1016/j.jclepro.2024.144452.
[29] Kowalik J, Tworek M. Properties of acrylic dispersions and coatings modified with ionic liquid. *Journal of Dispersion Science and Technology*, **2025**, *7*, 1-10. 10.1080/01932691.2025.2527268.
[30] Fu L, Ren Z, Chen W, et al. Polyetheramine enhanced biosurfactant/biopolymer flooding for enhanced oil recovery. *Journal of Molecular Liquids*, **2024**, *411*, 125757. 10.1016/j.molliq.2024.125757.
[31] Noor S, Taj M B, Ashar A. Solubilization of cationic dye in single and mixed micellar media. *Journal of Molecular Liquids*, **2021**, *330*, 115613. 10.1016/j.molliq.2021.115613.
[32] Wang Q, Zhang X, Wang W, et al. Gas-liquid interface properties of fluorocarbon and hydrocarbon surfactants and their mixed foams: molecular dynamics simulations and experimental studies. *Journal of Environmental Chemical Engineering*, **2024**, *12*, 114685. 10.1016/j.jece.2024.114685.
[33] Luo R, Miao J, Zhao Y, et al. The swelling mechanism of ethylene-vinyl acetate polymer

in different solvents via molecular dynamics and experimental studies. *Soft Matter*, **2025**, *21*, 708-18. 10.1039/d4sm01061b.
[34] Bidoire L, Vermant J. Mapping out the interplay between surfactant induced forces in thin liquid films. *Communications Physics*, **2025**, *8*, 455. 10.1038/s42005-025-02410-9.
[35] Jiang W X, Duan J T, Feng L F, et al. Water as a medium for microwave-assisted grafting of maleic anhydride onto a PP film to improve its adhesion with a polyamide 6 film. *Chemical Engineering and Processing-Process Intensification*, **2023**, *190*, 109428. 10.1016/j.cep.2023.109428.
[36] Zhang M, Xin Y. Micro-mechanism research into molecular chains orientation synergistically induced by carbon nanotube and shear flow in injection molding. *Applied Sciences*, **2020**, *10(2)*:723. 10.3390/app10020723.
[37] Zhang X, Su T, Liu T, et al. Superior yield strength and high-tensile-toughness matching of medium-mn steel with gradient structure developed by cyclic torsion. *Steel Research International*, **2024**, *95*, 2300654. 10.1002/srin.202300654.
[38] Sang R, Yang F. Effect of TiO2@CaCO3 waterborne primer on the coloring performance of inkjet-printed wood product coatings. *Coatings*, **2023**, *13*, 2071. 10.3390/coatings13122071.
[39] Peng Y, Musah M, Via B, et al. Calcium carbonate particles filled homopolymer PP at different loading levels: mechanical properties characterization and materials failure analysis. *Journal of Composites Science*, **2021**, *5*, 302. 10.3390/jcs5110302.
[40] Hibi Y, Uesaka S, Hitomi K, et al. A nearly zero-cost lot-by-lot inspection of recycled plastics: prediction of mechanical properties from viscosity evolution during melt kneading. *ACS Sustainable Resource Management*, **2025**, *2*, 673-6780. 10.1021/acssusresmgt.5c00040.
[41] Zhang Z, Xiang P, Zhang Z, et al. Preparation of high-performance water-based ink from acrylic-modified rosin resin. *Dyes and Pigments*, **2024**, *231*, 112401. 10.1016/j.dyepig.2024.112401.
[42] Chen X, Rossi D, Guo Y, et al. Effect of corona treatment on the adhesion between a two-component polyurethane adhesive and PP. *Macromolecules*, **2024**, *57*, 6646-6656. 10.1021/acs.macromol.4c00897.

Supplementary Files

This is a list of supplementary files associated with this preprint. Click to download.

- SupportingInformation.docx